Bull. Min. Res. Exp. (2018) 157: 1-21

Bulletin of the Mineral Research and Exploration

http://bulletin.mta.gov.tr

Geochemical and petrologic evolution of Otlakbaşı basaltic volcanism to the east of Lake Van

Vural OYAN[a*]

[a]*Yüzüncü Yıl University, Faculty of Engineering, Department of Mining Engineering, 65080, Van. orcid.org/0000-0002-1566-9749*

Research Article

Keywords:
Eastern Anatolia, Otlakbaşı volcanism, crustal contamination, partial melting, spinel peridotite.

ABSTRACT

Collision-related Otlakbaşı volcanism to the east of Lake Van occurred by eruptions from extensional fissures. In this study, new Ar-Ar age data and major, trace and rare earth elements characteristics of the Otlakbaşı basaltic volcanism are investigated. The Ar-Ar age data indicate that this basaltic volcanism erupted in Early Pliocene time in contrast to its previously known as Quaternary age. The volcanic products are basaltic composition and close to alkaline-subalkaline division line. Results of fractional crystallization accompanied by assimilation (AFC) modelling imply that fractional crystallisation can be negligible compared to crustal contamination in the evolution processes of the magma chamber and ratio of the crustal contamination to the fractional crystallisation (r values) varies from 0.1 to 0.35. Enrichment of large ion lithophile elements (LILE) and light rare earth elements (LREE) relative to high strength field elements (HFSE) and behaviour of mobile elements (Ba and Th) reveal that the mantle source region of the Otlakbaşı basaltic volcanism might have been enriched by melts that were derived from subducted sediments. Depletion in Rb and K elements of the fractionated-corrected samples indicate that amphibole and/or phlogopite could be presence in the mantle source. Results of partial melting model studies show that this basaltic volcanism can be predominantly produced by the melting of the spinel peridotite source. Metasomatized spinel bearing lithospheric mantle may be responsible for the eruption of the Otlakbaşı basaltic volcanism.

Received Date: 07.12.2017
Accepted Date: 04.02.2018

1. Introduction

Turkey is located within geodynamic belts coeval with collision, post collision and arc in the collision zone between the Gondwana and Eurasian plates. As a result, it appears to be a natural laboratory in terms of geological variety. The East Anatolian Collision Zone (EACZ) is a high plateau formed by north-south compression linked to continental collision in the stage from the Miocene on, following subduction of the Tethys ocean between the Arabian and Eurasian plates (Şengör and Kidd, 1979). As a result of this collision east-west oriented folds, reverse faults, and the strike-slip North Anatolian and East Anatolian fault systems (Figure 1a) developed in the region (Yılmaz et al., 1987). The EACZ is characterised by volcanic activity ranging from the Miocene to historical periods (Keskin et al., 2013; Oyan et al., 2016, 2017). This volcanic activity began in the south of the EACZ before 15 My (Lebedev et al., 2010). Recent studies indicate the last oceanic lithosphere in the East Anatolian region was completely subducted before 20 My (Okay et al., 2010). Additionally, Karaoğlan et al. (2016) emphasised that the collision between the Taurides and Anatolian plates occurred in the Oligocene. The tectonic regime in East Anatolia was characterised by compression-contraction until the end of the Late Miocene and Early Pliocene, then transformed to a compressional-extension in the Early-Late Pliocene (Koçyiğit et al., 2001). Many researchers have proposed different geodynamic models for the East Anatolian region and different sources for volcanism extending over large areas of the region (İnnocenti et al., 1982; Pearce et al., 1990; Keskin et al., 1998; Yılmaz et al., 1998; Keskin, 2003; Şengör et al., 2008; Allen and Armstrong, 2008; Schildgen

* *Corresponding author: Vural OYAN, vuraloyan@yyu.edu.tr*
http://dx.doi.org/10.19111/bulletinofmre.427782

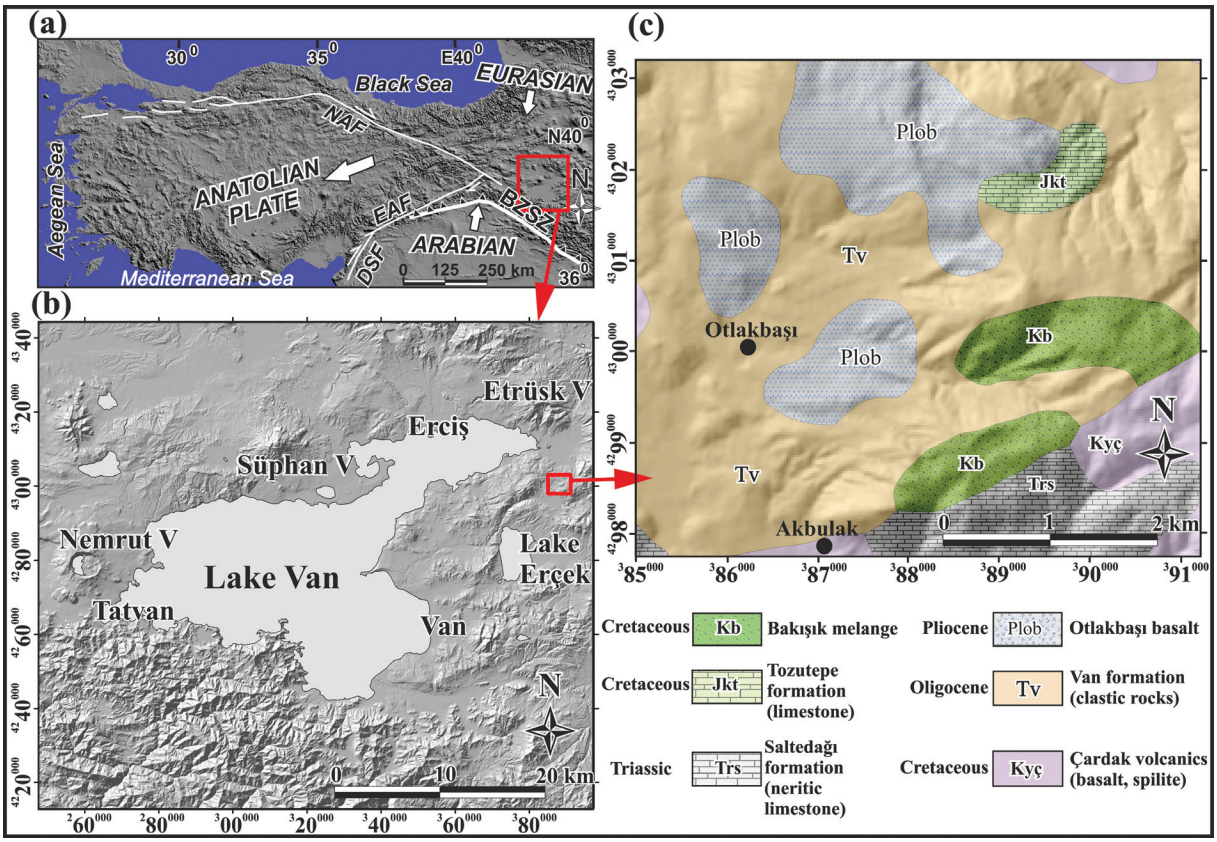

Figure 1- Location and geology maps for Otlakbaşı volcanism, a) Main neotectonic lineations in Turkey, b) Large volcanic centres in Lake Van basin and the study area (marked in red), c) Geology map of the study area (MTA, 2008, adapted from the geological report for 1/100000 scale K-51 sheet).

et al., 2014). The most important models proposed for the geodynamic evolution of the region are (1) lithospheric delamination (Pearce et al., 1990; Keskin et al., 1998); (2) oceanic crust becoming vertical and slab break-off (Keskin, 2003; Şengör et al., 2008) and (3) oceanic slab rupture (Allen and Armstrong, 2008; Schildgen et al., 2014). Studies in recent years have revealed that the volcanic activity observed in large areas on a regional scale may have formed by mixing of melts derived from lithospheric and asthenospheric mantle with different degrees of melting (Özdemir and Güleç, 2014; Oyan et al., 2016). The volcanic activity in the region reached a peak in the Pliocene, and continued with reducing volumes until the Quaternary (Oyan et al., 2016). This magmatic activity observed in the interval from the Pliocene to the Pleistocene formed volcanic centres like Nemrut, Süphan, Ağrı, Tendürek and Etrüsk (Figure 1b) and large regional-scale plateaus or basaltic lava flows locally along extensional fractures.

The Otlakbaşı lava located east of Lake Van (Figure 1) formed as lava erupting from extensional fractures. The Otlakbaşı lava cuts Cretaceous-aged limestone and Oligocene-aged clastic rocks and covers both these units and the Cretaceous ophiolite units observed over large areas in the region and Triassic-aged limestones.

In this study the aims were *(1)* to present new geochronologic, geochemical and petrologic data belonging to the Otlakbaşı volcanism east of Lake Van, *(2)* to discuss data obtained from petrologic modelling studies with magma chamber evolution processes, the nature of the mantle source area and melt processes and *(3)* to assess findings associated with regional geodynamic processes.

2. Regional Geology

The basement of the Anatolian-Iranian platform within the EACZ comprises microterranes amalgamated from the Late Cretaceous-Early Tertiary (Şengör, 1979). These microterranes are separated by ophiolitic complexes and adhesion complexes. There are 5 different tectonic blocks defined in East

Anatolia. There are *(1)* Rhodope-Pontide unit to the northeast of the region (Topuz et al., 2004); *(2)* the northwest Iran section (Karapetian et al., 2001); *(3)* the East Anatolian Accretionary Complex located between the Aras River and Bitlis-Pötürge massif (EAAC) (Şengör et al., 2008); *(4)* the Bitlis-Pötürge massif located along the Tauride belt (Şengör et al., 2008); and *(5)* the Arabian continent or autochthonous units ahead of it (Şengör et al., 2008; Keskin, 2007).

Following block uplift within the EACZ volcanism began before 15 My (Lebedev et al., 2010) with lava flows and pyroclastic products outcropping widely in the region. This volcanic activity produced three different types of eruption dynamics (effusive, extrusive, explosive). These volcanic units covered the tectonic blocks within the EACZ masking them, with volcanic products covering nearly 2/3 of the region and locally reaching 1 km thickness (Keskin, 2007).

Geophysical studies to reveal the crustal structure and geodynamic processes in the EACZ indicate the area between the Aras River and the Bitlis-Pötürge Massif has no lithospheric mantle and the East Anatolian Accretionary Complex (EAAC; Şengör et al., 2008) sits direction on asthenospheric mantle (Al-Lazki et al., 2003; Sandvol et al., 2003). As a result of geodynamic evolution, the crustal thickness is 38 km in the south section of the East Anatolian region, while it reaches 50 km in the northern section (Zor et al., 2003). In light of this data, Keskin (2003) stated the Neotethyan oceanic lithosphere ruptured while sinking into the asthenosphere and that volcanism with character varying from calc-alkali to alkali in the region may have developed due to this mechanism.

Recently some geophysical studies have indicated there may be 25-30 km of lithospheric mantle below the East Anatolia region and that the lithosphere may reach 70-75 km thickness (Angus et al., 2006; Özacar et al., 2008).

The EACZ transitioned to a compressional-extensional tectonic regime in the Early-Late Pliocene (Koçyiğit et al., 2001) and it is known that some zones of the crust displayed clear compression-thickening while other zones display extension-thinning characteristics as a result of delamination of the region below the lithospheric mantle (Göğüş and Pysklywec, 2008). Regionally, the Early Pliocene volcanism is known to have formed due to partial delamination of the lithospheric mantle (Pearce et al., 1990). Studies in recent years have revealed that volcanism began before 15 My (Lebedev et al., 2010; Oyan, 2011); additionally, a peak was reached nearly 5 My ago in terms of volume of erupted material and at this point basaltic lava forming widespread plateaus erupted in the region (Oyan, 2011). Within the scope of this study, the petrologic evolution, geochemistry and Ar-Ar age dates are presented for the rocks of the Otlakbaşı volcanism, a product of Pliocene basaltic volcanism, for the first time.

3. Analytic Techniques

Rock samples taken during field studies were prepared for petrographic, geochemical and Ar-Ar geochronologic dating analyses. Samples were first cut using a Struers brand diamond cutting disk. Cut rock samples had 30-micron thickness thin sections made for mineralogic petrographic analyses and were investigated under a polarising microscope. For geochemical analyses, samples first had the outer sections cleaned of dust, soil, moss and secondary formations. Later, a jaw crusher was used to break samples and they were powdered with the aid of an agate mortar and prepared for analysis.

Geochemical main oxides, trace elements and rare earth element analyses were performed in Acme Analytic Laboratories (Acme Labs) in Canada. Main element analyses were measured using an inductively-coupled plasma emission spectrometer (ICP-OES) with the lithium metaborate/tetraborate fusion technique. The detection limits for main elements varied from 0.001 to 0.04%. Loss on ignition (LOI) was determined with the firing method for sample separation and later obtained by measuring weight loss. For trace and rare earth element (REE) analyses, 0.2 g samples were mixed with $LiBO_2/Li_2B_4O_7$ in graphite crucibles. The prepared crucibles were fired in an oven. Later, melted samples were dissolved in 5% HNO_3 and trace element and rare earth element analyses were completed with an inductively-coupled plasma mass spectrometer (ICP-MS). For reliability of data obtained from main, trace and rare earth element analyses, standards for the analysis laboratory (reference material SO-18) were analysed at the same time as the samples. For standard SO-18, trace and rare earth elements, deviation of 5% or better was obtained. The main oxide, trace element and rare earth element results for rock samples from the Otlakbaşı volcanics and laboratory standards are given in table 1.

Table 1- Main oxides, trace elements and rare earth element analysis results for Otlakbaşı basaltic rocks.

Sample No	2015-5	2015-11	2015-12	2015-13	2015-14	2015-16	2015-19	2015-23	2015-25
Rock Type	*Basalt*	*Basalt*	*Basalt*	*Basalt*	*Basalt*	*Basalt*	*Basalt*	*Basalt*	*Basalt*
Coordinates (UTM)	***N:***4331972 ***E:***364899	***N:***4331972 ***E:***364899	***N:***4331972 ***E:***364899	***N:***4331972 ***E:***364899	***N:***4331972 ***E:***364899	***N:***4331972 ***E:***364899	***N:***4331972 ***E:***364899	***N:***4331972 ***E:***364899	***N:***4331972 ***E:***364899
SiO_2 ***%***	47.63	48.35	48.24	48.28	48.23	47.70	48.43	49.02	49.04
TiO_2	1.28	1.35	1.33	1.32	1.36	1.32	1.28	1.26	1.27
Al_2O_3	17.02	16.95	17.16	17.05	16.92	16.97	16.99	17.14	17.03
$Fe_2O_3^{TOT}$	9.47	9.62	9.64	9.52	9.74	9.42	9.13	9.17	9.19
MnO	0.16	0.16	0.15	0.15	0.16	0.16	0.15	0.16	0.15
MgO	8.77	8.26	8.39	8.34	8.35	7.59	7.55	7.13	7.76
CaO	10.85	10.35	10.38	10.59	10.25	11.08	11.13	11.27	10.89
Na_2O	3.10	3.14	3.16	3.11	3.20	3.13	3.17	3.04	3.22
K_2O	0.59	0.53	0.61	0.60	0.51	0.61	0.80	0.83	0.86
P_2O_5	0.21	0.22	0.24	0.22	0.21	0.23	0.25	0.25	0.26
LOI	0.6	0.7	0.4	0.5	0.8	1.5	0.8	0.4	0.0
Total	99.71	99.73	99.72	99.72	99.73	99.74	99.73	99.71	99.71
Mg#	0.732	0.717	0.721	0.722	0.717	0.704	0.712	0.699	0.718
V ***(ppm)***	189	193	196	186	187	193	196	205	199
Co	40.7	42.2	40.5	39.3	39.2	38.1	32.5	36.4	35.7
Ni	94.5	93.3	94.7	93.8	92.0	75.2	51.9	58.2	58.8
Sr	404.6	346.2	389.1	374.8	347.3	361.7	442.9	493.3	488.0
Rb	12.1	7.7	11.5	11.8	8.1	11.3	16.1	15.5	18.7
Ba	214	261	223	297	165	223	242	353	279
Th	2.0	1.8	2.1	2.1	1.7	2.0	2.6	3.1	3.3
Ta	0.4	0.3	0.4	0.4	0.3	0.3	0.3	0.4	0.5
Nb	5.6	5.1	6.1	6.9	4.7	5.5	6.5	7.2	7.4
Zr	126.6	129.6	118.9	119.8	128.2	114.7	123.3	131.9	131.8
Y	23.8	25.3	23.5	24.4	22.7	22.7	22.2	24.9	24.7
Hf	3.3	3.1	2.7	2.9	3.2	2.7	2.8	3.0	3.5
U	0.4	0.4	0.5	0.6	0.4	0.4	0.5	0.6	0.6
Pb	2.2	2.2	1.2	1.7	0.7	0.8	2.6	3.1	2.6
La	15.0	11.8	13.8	14.6	11.4	13.4	18.8	20.6	21.2
Ce	31.6	24.4	28.6	31.2	24.0	27.6	37.8	42.0	43.0
Pr	4.15	3.61	3.70	3.98	3.42	3.76	4.82	5.44	5.51
Nd	17.3	15.3	16.1	16.6	14.7	15.5	21.0	22.3	23.2
Sm	3.85	3.90	3.69	3.94	3.86	3.70	4.51	4.88	4.93
Eu	1.33	1.30	1.26	1.35	1.27	1.24	1.45	1.59	1.60
Gd	4.53	4.47	4.42	4.56	4.22	4.13	4.62	5.09	5.05
Tb	0.73	0.75	0.70	0.75	0.73	0.68	0.71	0.77	0.82
Dy	4.45	4.42	4.60	4.25	4.49	4.21	4.19	4.38	4.64
Ho	0.93	0.96	0.96	0.87	0.98	0.92	0.87	0.94	0.99
Er	2.74	2.70	2.65	2.93	2.68	2.46	2.56	2.66	2.68
Tm	0.40	0.39	0.37	0.41	0.38	0.37	0.37	0.41	0.43
Yb	2.36	2.54	2.66	2.62	2.58	2.25	2.54	2.70	2.55
Lu	0.38	0.39	0.41	0.41	0.40	0.38	0.37	0.42	0.42
CIPW									
Quartz	0	0	0	0	0	0	0	0	0
Orthoclase	3.54	3.185	3.652	3.599	3.067	3.694	4.81	4.97	5.13
Albite	24.624	27.035	27.103	26.705	27.551	26.086	26.063	26.07	27.126
Anorthite	31.27	31.123	31.258	31.244	30.829	31.206	30.286	31.09	29.755
Nepheline	1.095	0	0	0	0	0.573	0.669	0	0.203
Diopside	17.58	15.711	15.463	16.469	15.598	18.878	19.38	19.158	18.429
Hiperstene	0	3.745	1.367	1.522	2.651	0	0	2.345	0
Olivine	14.36	11.388	13.332	12.767	12.432	11.842	11.193	8.812	11.719
Magnetite	4.568	4.684	4.7	4.63	4.748	4.603	4.536	4.542	4.594
Ilmenite	2.469	2.61	2.56	2.545	2.628	2.57	2.473	2.425	2.435

Table 1- continued.

Sample No	***2015-27***	***2015-29***	***2015-30***	***2015-32***	***2015-33***	***2015-34***	*SO-18*	*SO-18*	*SO-18*
Rock Type	*Basalt*	*Basalt*	*Basalt*	*Basalt*	*Basalt*	*Basalt*	*Standard*	*Standard*	*Standard*
Coordinates (UTM)	***N:***4331972 ***E:***364899	***N:***4331972 ***E:***364899	***N:***4331972 ***E:***364899	***N:***4331972 ***E:***364899	***N:***4331972 ***E:***364899	***N:***4331972 ***E:***364899	*Analysed*	*Analysed*	*Expected values*
SiO_2 **%**	48.49	48.84	48.17	47.98	48.84	48.44	58.1	58.08	58.09
TiO_2	1.27	1.28	1.33	1.29	1.29	1.31	0.69	0.69	0.69
Al_2O_3	16.90	17.03	17.05	17.01	17.04	17.04	14.13	14.13	14.13
$Fe_2O_3^{TOT}$	8.99	9.17	9.65	9.43	9.49	9.56	7.61	7.61	7.6
MnO	0.15	0.15	0.15	0.15	0.15	0.15	0.39	0.39	0.39
MgO	7.29	7.46	8.26	8.53	8.50	8.04	3.33	3.33	3.33
CaO	11.45	11.18	10.34	10.31	10.32	10.28	6.36	6.37	6.37
Na_2O	3.11	3.05	3.27	3.25	3.19	3.28	3.68	3.68	3.69
K_2O	0.85	0.84	0.57	0.55	0.63	0.54	2.15	2.15	2.16
P_2O_5	0.27	0.26	0.22	0.20	0.22	0.21	0.82	0.83	0.83
LOI	0.9	0.4	0.7	1.0	0.0	0.8	1.9	1.9	1.9
Total	99.70	99.72	99.72	99.71	99.72	99.71	99.72	99.72	99.72
Mg#	0.708	0.708	0.718	0.728	0.727	0.714			
V ***(ppm)***	200	199	189	177	189	183	198	198	199
Co	33.8	36.2	43.6	42.4	40.3	42.3	26.2	26.1	26.2
Ni	56.2	49.2	99.1	99.1	73.1	104.1	40	46	44
Sr	481.3	492.9	362.4	354.2	378.5	375.2	399.1	400.1	403
Rb	16.5	16.7	9.8	10.5	12.7	10.0	28	28	28.2
Ba	317	334	193	338	208	372	496	497	498
Th	3.3	3.2	2.2	1.6	2.2	1.9	9.7	9.8	9.7
Ta	0.4	0.5	0.5	0.4	0.4	0.3	7.2	7.2	7.1
Nb	7.4	8.0	5.7	4.6	6.2	5.2	21.2	20.8	21
Zr	130.3	134.6	125.8	126.3	116.8	132.1	281.5	279.9	280.8
Y	24.6	24.1	25.3	22.8	24.4	25.0	31.5	31.3	31.3
Hf	3.3	3.1	2.8	3.1	2.9	3.2	9.6	9.7	9.4
U	0.6	0.9	0.4	0.5	0.4	0.4	16	16.1	16.1
Pb	3.3	2.5	0.5	1.7	2.0	1.9			
La	20.6	20.6	14.4	12.5	14.7	12.1	11.9	11.8	12
Ce	41.2	41.6	28.5	25.6	29.6	25.8	26.5	26.9	27
Pr	5.42	5.58	3.88	3.54	4.01	3.61	3.4	3.39	3.39
Nd	22.3	21.7	16.6	15.5	17.4	15.8	13.9	13.8	13.8
Sm	4.83	5.06	3.89	3.66	4.33	3.75	2.86	2.81	2.89
Eu	1.45	1.59	1.43	1.24	1.27	1.34	0.87	0.86	0.86
Gd	5.18	5.07	4.61	4.50	4.46	4.39	2.85	2.85	2.83
Tb	0.81	0.82	0.77	0.75	0.72	0.72	0.5	0.5	0.5
Dy	4.62	4.89	4.66	4.52	4.44	4.43	2.9	2.86	2.92
Ho	0.93	0.98	0.93	0.97	0.95	0.90	0.61	0.6	0.6
Er	2.66	2.81	2.73	2.74	2.71	2.72	1.79	1.77	1.79
Tm	0.42	0.41	0.42	0.40	0.40	0.41	0.28	0.28	0.28
Yb	2.55	2.76	2.63	2.48	2.74	2.60	1.74	1.75	1.76
Lu	0.39	0.41	0.39	0.37	0.40	0.38	0.27	0.26	0.26
CIPW									
Quartz	0	0	0	0	0	0			
Orthoclase	5.118	5.029	3.422	3.315	3.758	3.25			
Albite	25.518	26.164	28.127	27.689	27.255	28.262			
Anorthite	30.191	30.71	30.663	30.794	30.611	30.724			
Nepheline	0.698	0	0	0.191	0	0			
Diopside	20.691	19.024	16.002	15.991	15.674	15.834			
Hiperstene	0	1.241	0.093	0	2.816	2.15			
Olivine	10.218	10.218	13.868	14.43	12.24	12.043			
Magnetite	4.471	4.538	4.735	4.619	4.657	4.707			
Ilmenite	2.458	2.465	2.568	2.498	2.473	2.534			

Ar-Ar dating analyses were performed in the isotope and geochronology laboratories of Nevada University (Las Vegas, United States of America). Samples for analysis were wrapped in Al foil and stacked in 6 mm internal diameter sealed fused silica tubes. Individual packets with mean 3 mm thickness were inserted with neutron flux monitors (FC-2, Fish Canyon tuff sanidine) at 5-10 mm intervals. The FC-2 sanidine standards heated together with CaF_2 and K-glass pieces were placed on a Cu sample tray in a high vacuum line and melted with a 20 W CO_2 laser. During the laser fusion, samples were imaged with a video camera system. Samples were analysed with the step-by-step heating method in a dual vacuum resistant oven similar to the design of Staudacher et al. (1978).

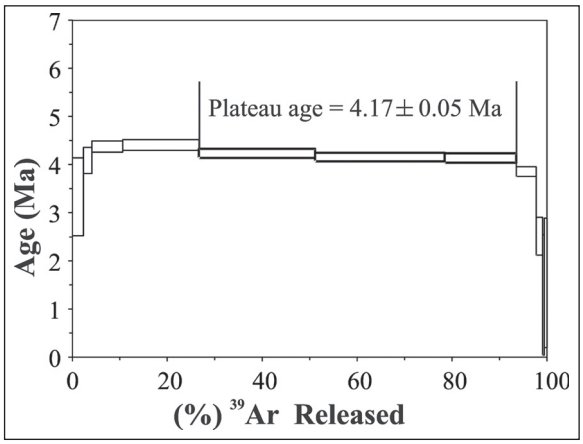

Figure 2- Ar-Ar plateau age for Otlakbaşı volcanic rocks. Best plateau formed between steps 4 and 7. Between these steps the ^{39}Ar amount released was 67%.

4. Results

4.1. Geology and Geochronology of the Area

Otlakbaşı lava comprises a basaltic-composition lava series erupted from different extensional fractures east of Lake Van. With outcrops in different locations, the Otlakbaşı lava covers a 4 km area at most and cuts clastic rocks called the Van formation (Acarlar et al., 1991) (Figure 1c). These clastic rocks comprise Oligocene-Miocene-aged sandstone, claystone and siltstone successions (Acarlar et al., 1991). The Otlakbaşı basaltic lava cuts Cretaceous-aged neritic limestones in the north of the study area (Figure 1c). This unit, called the Topuztepe formation, is formed of grey, white and dark grey colour limestone, dolomitic limestone and recrystallised limestone lithologies (Acarlar et al., 1991).

Within the study area, the Otlakbaşı lava flows unconformably overlie older ophiolitic melange units. Ophiolitic rock units are serpentinite, dunite and spilites. Covering all these lithologies, the Otlakbaşı volcanics cover a total area of nearly 15 km^2 (Figure 1c). Within rocks with black and grey colour, the largest observable feldspar and olivine microphenocrystals are nearly 0.5 cm in size.

A sample chosen to best represent the Otlakbaşı lava flow (Sample no: 2015-33) was sent for Ar-Ar dating analysis. The Ar-Ar geochronologic dating analysis of rock mass is in accordance with Ca/K. The analysed sample had total gas age of 4.14±0.004 My. Between steps 5-7, a plateau age of 4.17±0.05 My was defined (released 39Ar amount 67%) (Figure 2). Though an isochron age could not be determined for this sample, there were no alteration effects observed due to high radiogenic yield. The 4.17±0.05 My Ar-Ar age for Otlakbaşı lava indicates they erupted in the Early Pliocene (Zanclean), contrary to the known age of Quaternary. The age data belonging to the steps are given in table 2.

4.2. Mineralogy-Petrography

Rocks forming the Otlakbaşı volcanics are formed of plagioclase, olivine, pyroxene and opaque minerals (Figure 3). While olivines are observed as microphenocrystals and are iddingsitised, plagioclase phenocrystals have rod-like form, with polysynthetic twins observed. Some plagioclase microphenocrystals with cell-like structure developed were determined to have been eroded by magma along the edges. Colourless pyroxene crystals with microlith sizes, have lilac colour tones in some forms close to the titanaugite composition. Gas cavities observed in rocks are filled with secondary calcite and zeolite crystals. The groundmass of the Otlakbaşı rocks comprises microliths and volcanic glass. Generally, they display interstitial and flow textural characteristics. Glomeroporphyric texture characteristics formed by clusters of plagioclase, olivine and pyroxene minerals or plagioclase crystals were identified in the rocks (Figure 3).

4.3. Whole-rock Geochemistry

The freshest samples collected during fieldwork in locations where the Otlakbaşı volcanics outcrop were sent to ACME analytic laboratories in Canada for main oxide, trace element and rare earth element (REE) analyses. The results of analyses using ICP-AES and

Table 2- Apparent age data for steps in the Ar-Ar geochronologic dating analyses. T - temperature, My – million years, SE – standard error margin.

Step	T (^{0}C)	t (min.)	^{36}Ar	^{37}Ar	^{38}Ar	^{39}Ar	^{40}Ar	%^{40}Ar*	% ^{39}Ar	^{40}Ar*/^{39}Ar	Age (My)	1s.e.
1	560	12	0.791	0.305	0.281	7.503	228.015	3.6	2.3	1.075392	3.33	0.40
2	620	12	0.074	0.221	0.094	5.691	26.270	41.1	1.8	1.318518	4.08	0.14
3	680	12	0.071	0.647	0.281	20.928	47.161	75.0	6.5	1.411981	4.37	0.06
4	740	12	0.071	1.242	0.685	51.701	90.239	89.7	16.1	1.422654	4.40	0.06
5	800	12	0.082	1.598	1.049	78.776	127.168	90.2	24.5	1.366703	4.23	0.05
6	870	12	0.092	1.615	1.196	87.834	140.192	88.9	27.3	1.342125	4.16	0.04
7	960	12	0.092	1.005	0.695	48.507	89.309	81.7	15.1	1.335334	4.13	0.05
8	1050	12	0.109	0.928	0.292	13.554	46.317	47.1	4.2	1.243824	3.85	0.05
9	1140	12	0.136	0.627	0.136	4.298	41.850	12.7	1.3	0.811043	2.51	0.20
10	1230	12	0.171	0.263	0.068	1.190	48.898	1.4	0.4	0.417326	1.29	0.63
11	1400	12	0.487	0.463	0.147	1.850	137.305	0.8	0.6	0.497728	1.54	0.67
										Total gas age	4.14	0.04
										Plateau age	4.17	0.05

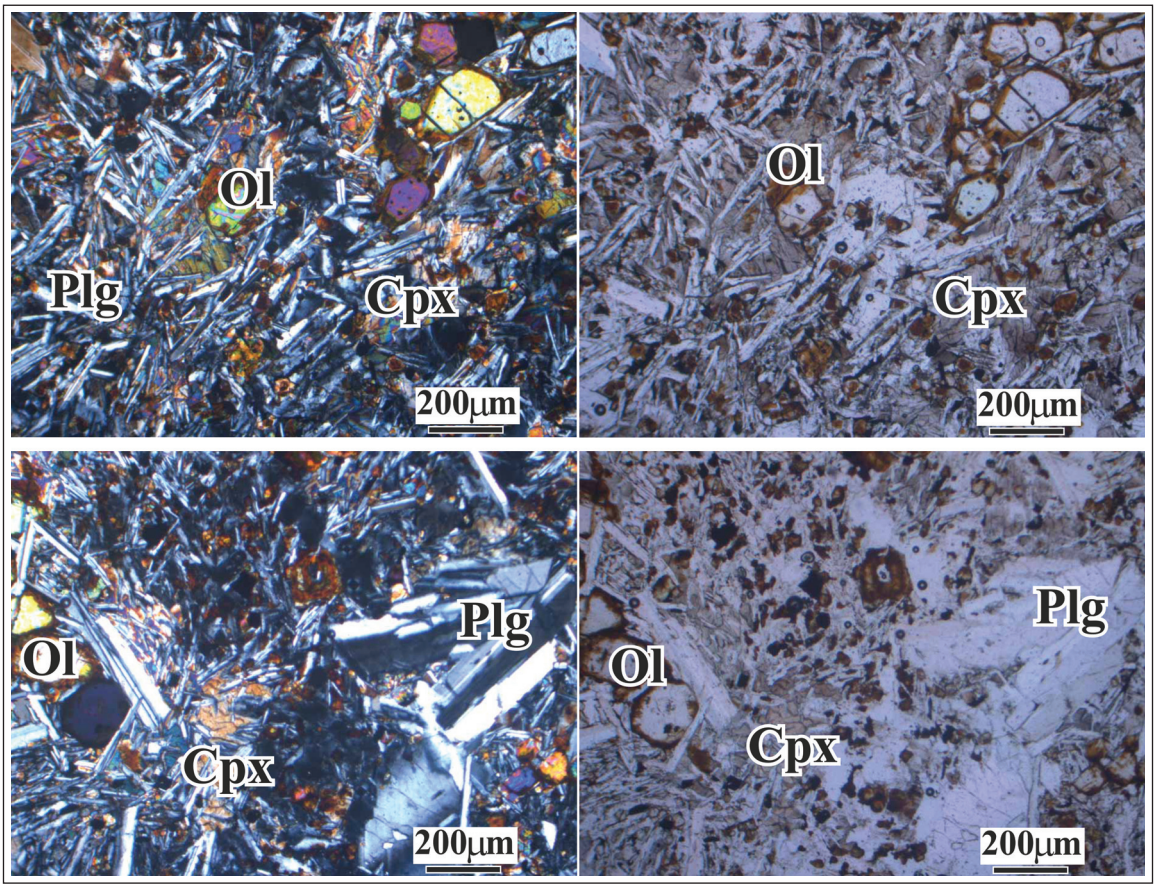

Figure 3- Thin section appearance of Otlakbaşı rocks. Distribution of iddingsitised olivine (Ol) phenocrysts and Ol, Cpx (clinopyroxene) and Plg (plagioclase) crystals in interstitial matrix

ICP-MS methods found low element mobility in rocks, with LOI (loss on ignition) values varying between 0 and 1, indicating that these rocks were fresh and not affected by alteration. Geochemical classification of these rocks was completed using values calculated for main oxide values on dry basis (distributing the water loss on ignition in proportion to the major element values). The lava erupted in the Otlakbaşı area fell in the basalt area on the total alkali (Na_2O+K_2O) – silica (TAS diagram; LeBas et al., 1986) classification diagram (Figure 4a).

With the aim of determining the character of the magma forming the rocks in the study area, the alkali-subalkali differentiation line of Irvine and Baragar (1971) was drawn on the TAS diagram and basalts fell close to the alkali-subalkali differentiation line and were located in the subalkali area. On the SiO_2 – K_2O diagram of Peccerillo and Taylor (1976), the rocks were located in the medium K series area (Figure 4b).

While the SiO_2 content of the Otlakbaşı basaltic samples varied in a narrow interval from 47.63-49.04%, the MgO contents varied from 7.13 to 8.77% with Mg# values varying from 0.699 to 0.732. As the SiO_2 content of the Otlakbaşı basaltic rocks varies in a narrow interval, they do not provide very clear information on the Harker variation diagrams. As a result, to produce more productive data for basaltic rocks on the Harker diagram the solidification index MgO values were used. The MgO binary Harker variation diagrams for some chosen main oxides are given in figure 5a and b. Though there are no very clear trends observed on MgO against main oxide variation diagram, there is a negative trend between MgO and SiO_2 and a positive trend with Fe_2O_3.

The MgO binary Harker variation diagrams for some trace elements from the basaltic samples are given in figure 5 c-f. Together with the fall in MgO in basaltic rocks, the Ni and Co elements have a negative trend, Sr and Y elements display close to horizontal or slightly positive trends. The traces of other trace elements and main oxide elements against MgO on Harker variation diagrams have irregular distribution or display completely horizontal trends.

The location of Otlakbaşı basaltic rock samples on primitive mantle (PM)-normalised multi-element diagrams is given in figure 6a. On these diagrams, all samples appear to be severely depleted in high field strength elements (HFSE), compared to large ion lithophile elements (LILE) and light rare earth elements (LREE). Samples presenting typical trends for active continental margin volcanism display enrichment in Pb and Sr compared to neighbouring elements. Medium and heavy rare earth elements in the primitive mantle-normalised rock samples are parallel to the PM line. The same samples on Sun and McDonough's (1989) chrondrite-normalised rare earth element (REE) spider diagrams (Figure 6b) display enrichment in all samples for LREE elements compared to medium rare earth elements (MREE) and heavy rare earth elements (HREE). The MREE and HREE plot parallel or close to parallel with primitive mantle values.

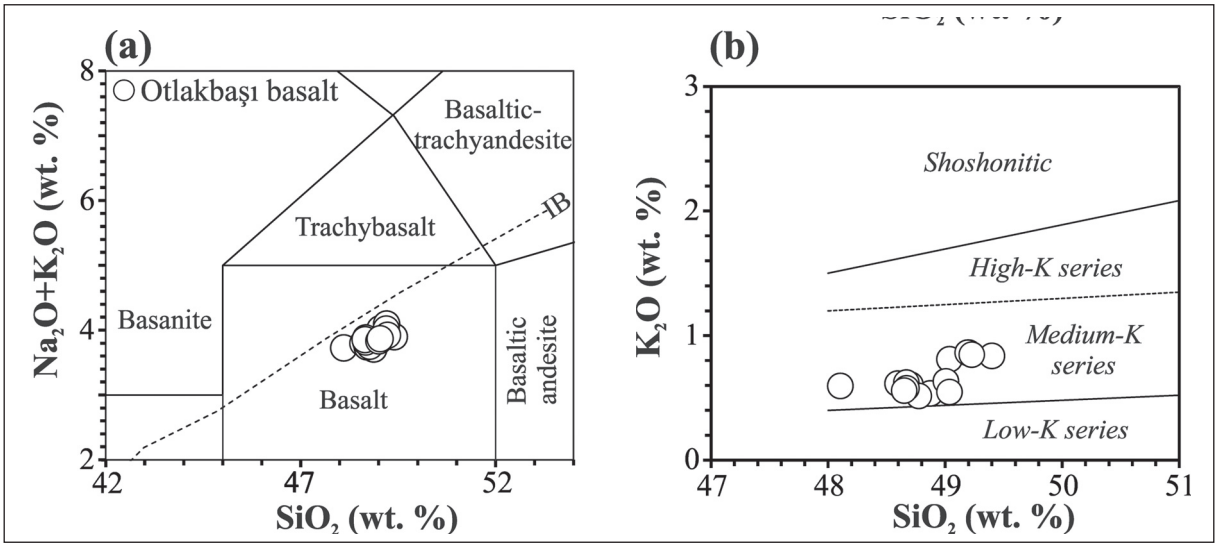

Figure 4- For Otlakbaşı volcanic rocks a) total alkali-silica (TAS: LeBas et al., 1986) classification diagram, b) SiO_2 (%)-K_2O (%) variation diagram (Peccerillo and Taylor, 1976).

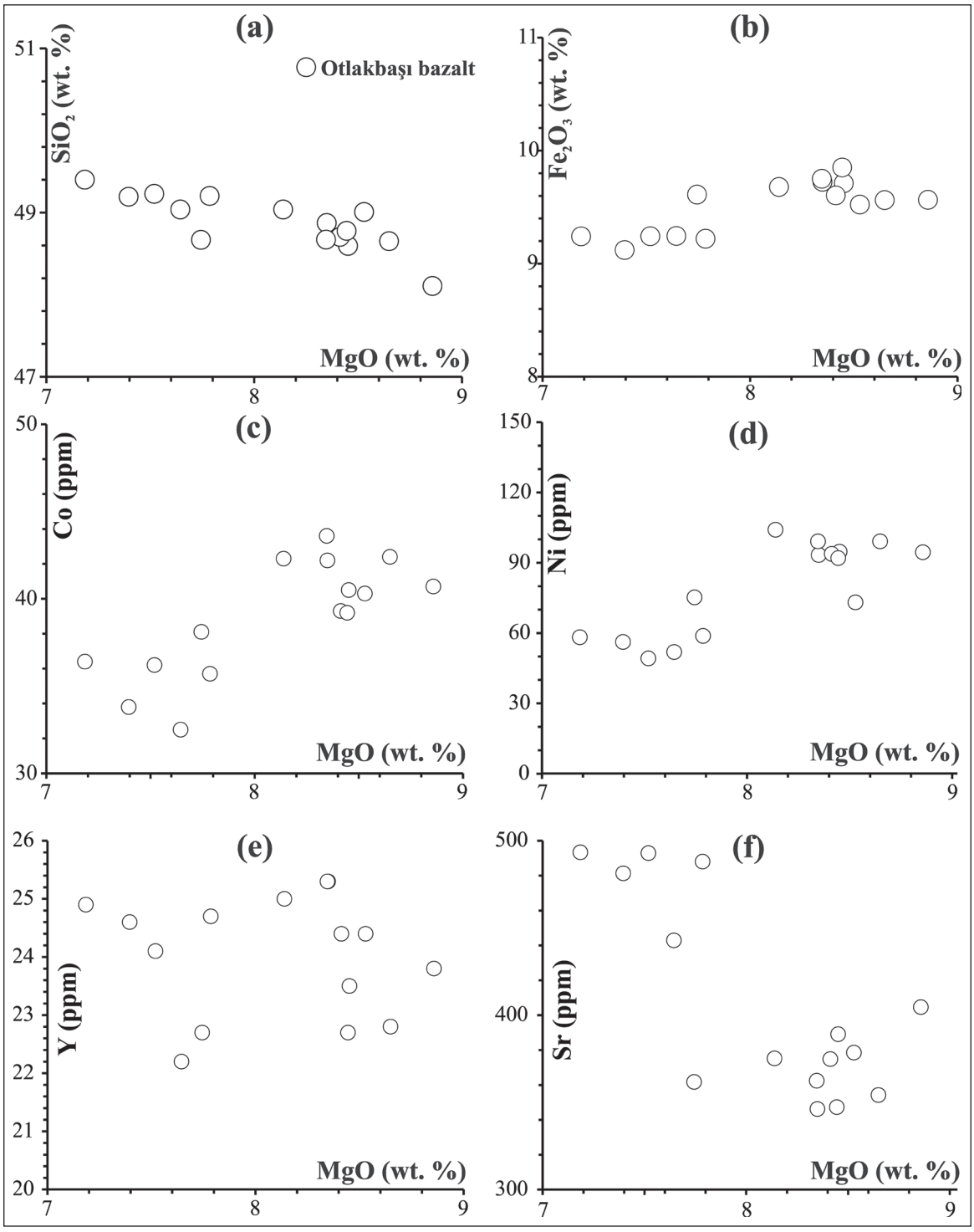

Figure 5- Selected main oxide and trace elements against MgO for Otlakbaşı basaltic rocks on Harker binary variation diagrams.

5. Discussion

5.1. Fractional Crystallisation

As the MgO and SiO_2 values for Otlakbaşı basaltic lava vary within a very narrow range on Harker variation diagrams against MgO values (Figure 5), the trends indicating fractional crystallisation could not be clearly observed. Only Fe_2O_3, Co and Ni had slightly positive trends against MgO, which indicates that the evolution of these rocks may have been partly affected by fractional crystallisation processes of

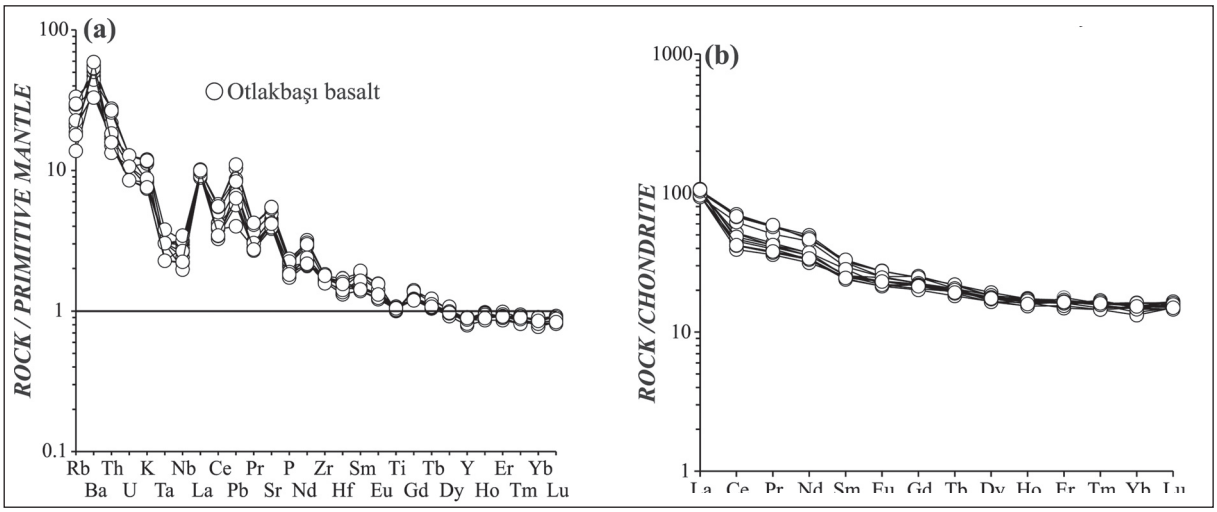

Figure 6- For Otlakbaşı basaltic lava a) multi element spider diagrams normalised to primitive mantle (PM), b) rare earth element (REE) spider diagrams normalised to chrondrite. Normalised values taken from Sun and McDonough (1989) for both diagrams.

ferromagnesian minerals like olivine and pyroxene. Together with the fall in MgO values, the slight increasing trend in SiO_2 indicates that fractional crystallisation may have affected the evolution of the rocks, though only slightly.

The positive trend of Y and Sr with MgO shows that amphibole and plagioclase were not affected by fractional crystallisation processes. To test whether fractional crystallisation was an effective evolutionary process for Otlakbaşı basaltic volcanism, Th-Co and Rb-Y binary variation diagrams were produced using the Rayleigh fractionation equation (Figure 7). On these diagrams, the fractional crystallisation trends for magmas with different mineralogic composition were drawn. On the Th against Co diagram for Otlakbaşı

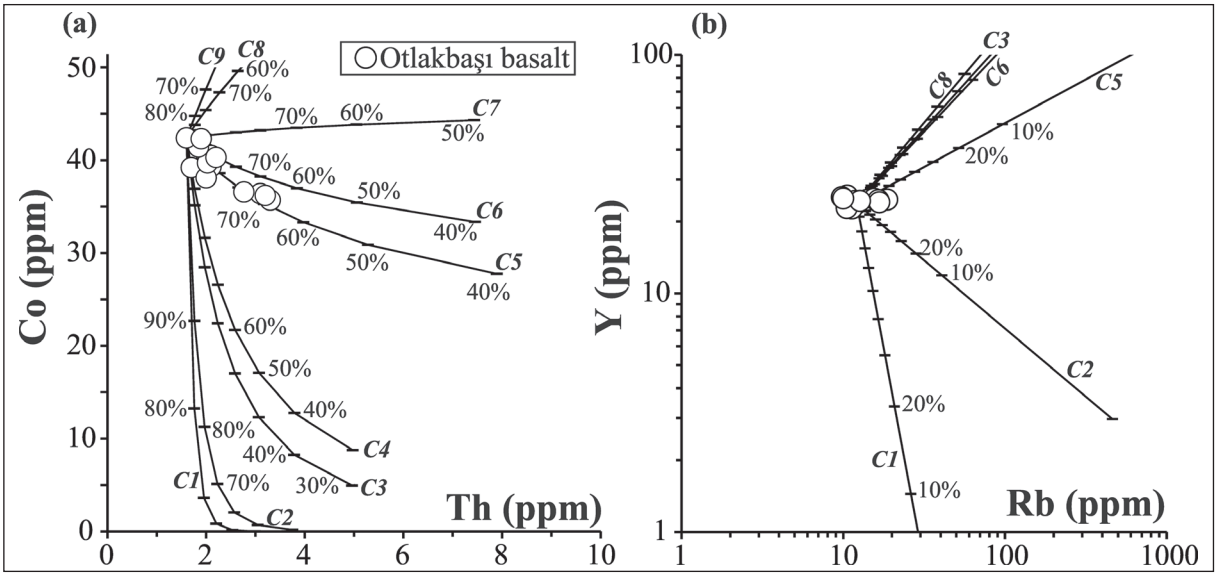

Figure 7- Co-Th normal – normal and Rb-Y log – log variation diagrams. Each curve modelled on the diagrams was calculated characterised by crystallisation of mineral assemblages given below according to Rayleigh crystallisation and traced on the diagram. % values given on the curves indicate post-crystallisation with remaining melt % indicated. ***C1***-$Amp_{0.2}$+$Plg_{0.5}$+$Cpx_{0.1}$+$Bio_{0.1}$+$Sn_{0.1}$, ***C2***-$Amp_{0.1}$+$Plg_{0.7}$+$Cpx_{0.1}$+$Bio_{0.05}$+$Sn_{0.05}$, ***C3***-$Plg_{0.5}$+$Cpx_{0.5}$, ***C4***-$Ol_{0.1}$+$Amp_{0.15}$+$Plg_{0.5}$+$Opx_{0.15}$+$Cpx_{0.1}$, ***C5***-$Ol_{0.2}$+$Plg_{0.6}$+$Cpx_{0.2}$, ***C6***-$Plg_{0.7}$+$Opx_{0.1}$+$Cpx_{0.2}$, ***C7***-$Amp_{0.1}$+$Plg_{0.65}$+$Bio_{0.05}$+$Sn_{0.1}$+$Cpx_{0.1}$, ***C8***- $Amp_{0.1}$+$Plg_{0.6}$+$Opx_{0.2}$+$Cpx_{0.1}$, ***C9***- $Plg_{0.5}$+$Opx_{0.5}$ (Amp; amphibole, Plg; plagioclase, Ol; olivine, Opx; orthopyroxene, Cpx; clinopyroxene, Bio; biotite, Sn; Sanidine). Discriminant coefficient values (Kd) used to obtain the curves taken from Geochemical Earth Reference website (http://www.earthref.org).

basaltic lava, the line falls on curves C5 and C6. This diagram shows that for magmatic systems comprising mineral assemblages of olivine (20%), plagioclase (60%) and clinopyroxene (20%), nearly 20% fractional crystallisation may create the Otlakbaşı lava. Additionally, for the fractional crystallisation model using Rb-Y elements, samples fall close to the C5 curve with 80% F value. This modelling clearly indicates that olivine and pyroxene minerals were affected by fractionation of the magma system, while crystallisation of other minerals was unimportant for Otlakbaşı basaltic volcanism.

5.2. Continental Contamination

Continental contamination processes occur as hot magma melts colder continental crust material and absorbs the material as it moves through the continental crust or while in a magma chamber and this event is reflected in the melt geochemistry (DePaolo, 1981). On multielement spider diagrams for Otlakbaşı basaltic lava (Figure 6a), there is clear enrichment of LILE and LREE compared to HFSE elements which may reflect the effects of continental contamination or continental contamination combined with fractional crystallisation (assimilation fractional crystallisation-AFC). Additionally, the Ta/Zr and Rb/Th element ratios are clearly enriched in continental crust compared to the mantle and are high in some Otlakbaşı basaltic lava samples. This data indicates that continental contamination may have been an effective process in the evolution of the Otlakbaşı volcanism. With the aim of revealing whether AFC effects were an important evolutionary process for Otlakbaşı basaltic lava, modelling studies were completed using DePaolo's (1981) AFC equations.

DePaolo's (1981) AFC modelling reveals the ratio of crustal contamination (M_a) to the ratio of fractional crystallisation (M_c) and this is shown as the assimilation fractional crystallisation ratio "r (M_a/M_c)". Another parameter used in these equations is the ratio of remaining magma mass after fractional crystallisation (M_m) to original magma (M_m^0) and is shown by "F (M_m / M_m^0)". With DePaolo's (1981) equations, curves may be modelled for different ***r*** values for trace element and isotope ratios and interpretations may be made about the true r value of rock samples. Rb, Th, Ta and Zr elements were used in the AFC modelling systematic derived for the Otlakbaşı basaltic lavas and different *r* values were produced with Rb-Rb/Th and Ta-Ta/Zr AFC modelling curves (Figure 8). With the crystallisation of the trace elements given above as some accessory minerals in acidic-character magmas, the Zr, Th and mica minerals, apart from Rb, are incompatible with minerals in most of the magma

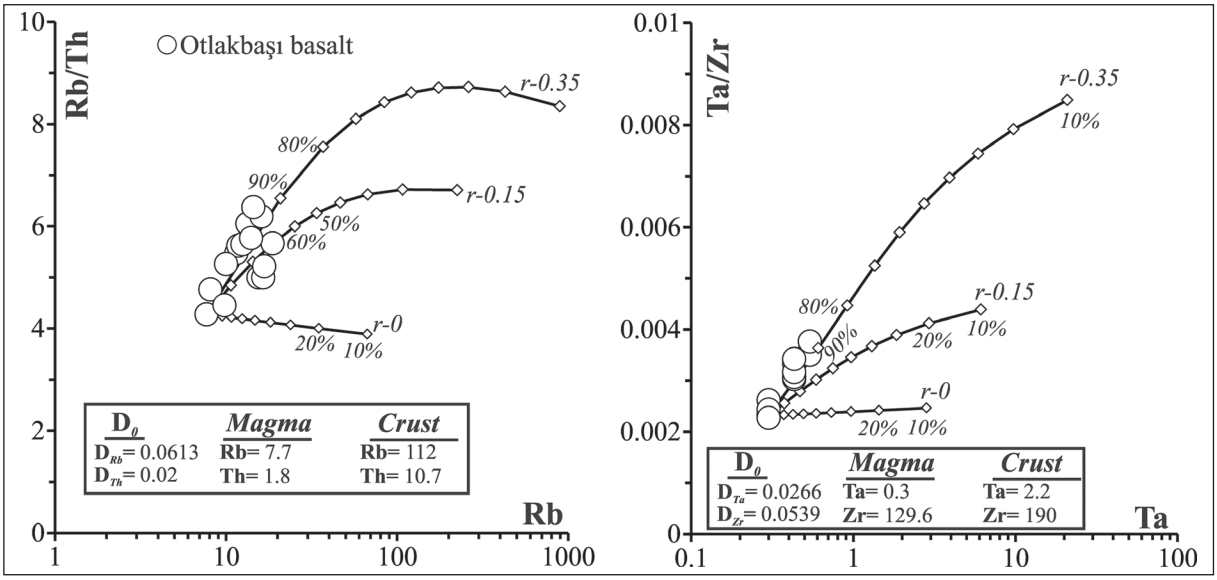

Figure 8- AFC modelling curves using DePaolo's (1981) equations. Values on the curves for r show the ratio of crustal contamination to fractional crystallisation. Percentage values on the model curves represent the F value of the original magma ratio in the residual magma mass after fractional crystallisation. The parameters used for formulation of modelling are given in the figure. Discriminant coefficient values taken from McKenzie and O'Nions (1991) and Adam and Green (2006). Total discriminant coefficients (D_0) for elements calculated on the basis of less evolved lava with olivine$_{(0.2)}$ +plagioclase$_{(0.6)}$ +clinopyroxene$_{(0.2)}$ mineralogic composition.

(D<<1). As a result, these trace elements are not affected by fractional crystallisation processes in most magma systems. Data presented in the mineralogy-petrography section and on figure 3 reveals the minerals mentioned above did not fractionate during the evolution of Otlakbaşı volcanism and that no differentiation process developed for these minerals. For these reasons, the variation in these elements and element ratios will be controlled by continental contamination. During Rb and Ta element modelling, fractionation indices, Ta/Zr and Rb/Th element ratios are selected as the continental contamination index and the samples were traced on binary variation diagrams for different r values (Figure 8).

As can be seen on figure 8, some of the basaltic rock samples fall along the curve with r values varying from 0-0.35. These samples, especially, are basaltic rocks with low MgO values reflecting the trace of continental contamination. Another noteworthy data point on the modelling curves is that fractional crystallisation varied from 0 to 10% for samples with low MgO values. This data indicates that for the Otlakbaşı basaltic lava, samples with low MgO values may have undergone an evolutionary process with significant continental contamination, but fractional crystallisation remained at negligible levels compared to continental contamination. Trends obtained from Harker variation diagrams that do not indicate fractional crystallisation are consistent with the data obtained from these modelling studies.

5.3. Mantle Source Area and Enrichment

On multielement spider diagrams normalised to primitive mantle, Otlakbaşı basaltic lava (Figure 6) is clearly depleted in Nb and Ta elements compared to neighbouring LILE and LREE, with clear enrichment in Pb, typically indicating the presence of subduction components in the mantle source area. Additionally, this effect may be reflected in the traces of continental contamination and fractional crystallisation in the magma chamber. In the magma chamber evolution processes of the Otlakbaşı basaltic volcanism, AFC processes play an effective role in samples with low MgO values with this effect not observed in samples with high MgO values. Due to these reasons, on multielement spider diagrams normalised to primitive mantle, the trends mentioned above reflect clear traces of subduction components for primitive lava with high MgO values in the Otlakbaşı volcanism. Ta/Yb – Th/Yb binary variation diagrams were produced with the aim of revealing the mantle source area of rock samples (Figure 9). Ta/Yb and Th/Yb ratios have nearly fixed values in asthenospheric mantle and small-volume melts derived from the asthenosphere and in enriched lithospheric mantle (Pearce et al., 1990). At the same time, Th and Ta elements with similar incompatibility have nearly the same differentiation coefficients in mantle melt and fractional crystallisation processes. High values for both Ta/Yb and Th/Yb elements indicates high degrees of mantle melting, with lavas with these values falling in the mantle area (or mantle metasomatisation) on source diagrams. However, sources containing subduction components or sources enriched in these components are enriched in Th and Ba elements, with increasing Th/Yb or Ba/Yb ratios deviating linked to the mantle area.

When figure 9 is examined, basaltic samples from the study area have increasing Th/Yb and nearly stable Ta/Yb values, with increasing Th/Yb ratios indicating they deviate from the mantle area. This data indicates

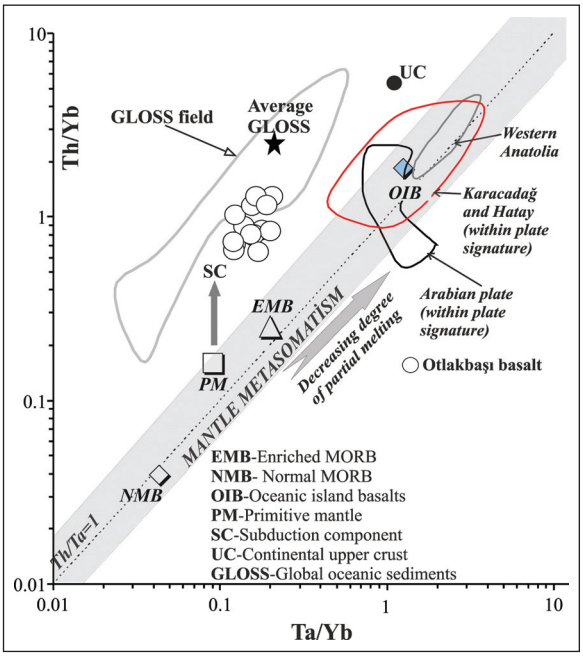

Figure 9- Location of Otlakbaşı basaltic lava on Ta/Yb-Th/Yb binary variation diagrams. PM, EMB, NMB and OIB values taken from Sun and McDonough (1989). UC and GLOSS (subducting oceanic sediment) values taken from Taylor and McLennan (1985) and Plank and Langmuir (1998), respectively. Values for the Arabian plate taken from Lustrino and Wilson (2007), Shaw et al. (2003) and Krienitz et al. (2006). Data for Karacadağ and Hatay taken from Keskin et al. (2012), Parlak et al. (2000) and Bağcı et al. (2011). Western Anatolia area taken from Aldanmaz et al. (2007). Mantle area shown on figures drawn according to values obtained from Pearce et al. (2005) and Sun and McDonough (1989).

the presence of subduction components in the mantle source area for the least evolved rock samples from Otlakbaşı basaltic volcanism. The process of adding subduction components into the mantle source area is described in two ways. These are (1) via the effects of fluids derived from altered oceanic crust (Tatsumi et al., 1986; Hawkesworth et al., 1997; Turner. 2002) or subducted sediments (Class et al., 2000; Elburg et al., 2002) or (2) via partial melting of altered oceanic crust or subducted sediments (Elliott et al., 1997; Hawkesworth et al., 1997). With these mechanisms, volcanic rocks erupting from magmas derived from enriched mantle have significant differences in their geochemical traces (Hawkesworth et al., 1997; Class et al., 2000; Foley et al., 2002; Kessel et al., 2005). Some LILE elements (Ba, Sr, Rb, U) are mobile in fluids, while HFSE and rare earth elements and Th are immobile in fluids but act in more mobile fashion in sediment or altered oceanic crust melts (Turner, 2002; Elburg et al., 2002; Foley et al., 2002; Kessel et al., 2005). As a result, ratios of elements enriched in fluid phase or sediment (or altered oceanic crust) melts may be used to determine enrichment processes in the source area. With this aim, Ba/Yb and Th/Yb binary variation diagrams recommended by Oyan et al. (2017) were produced (Figure 10). While Th is mobile in sediment or altered oceanic crust melts, Ba is mobile and enriched in the fluids released from these. Yb acts immobile in both cases, so slightly increasing Ba/Yb ratios compared to Th/Yb ratios indicate enrichment with fluids or metasomatisation processes, while Th/Yb ratios slightly increased compared to Ba/Yb ratios indicates enrichment processes with sediment melts. Situations when both values are low reflect melting or altered oceanic crust or metasomatisation processes with fluids released from this (Oyan et al., 2017). As seen in figure 10, the Otlakbaşı basaltic lava samples trend towards increasing Th/Yb ratios and reflect enrichment with dominantly sediment melts and metasomatisation processes. However, it should be noted that some samples fall between the curves for fluid from sediment (SF) and sediment melts (SM) and this indicates that metasomatisation processes with low rates (compared to sediment melts) of enrichment from fluids derived from sediments may have been effective. Another noteworthy trend is that some samples fall between primitive mantle and upper crust composition. As discussed in the continental contamination section, this complies with the continental contamination effects during the evolution of Otlakbaşı basaltic volcanism.

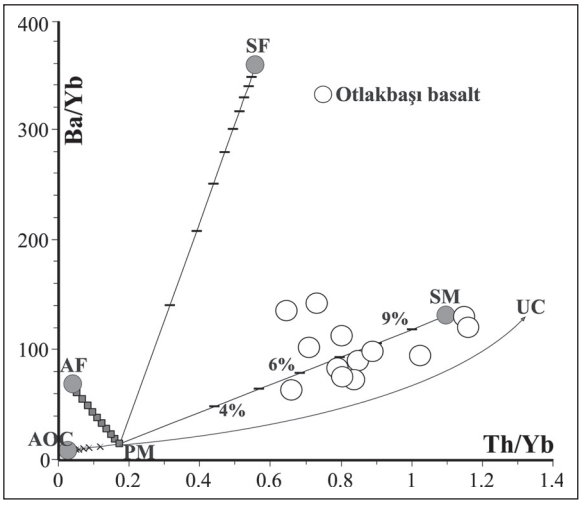

Figure 10- Th/Yb-Ba/Yb (Oyan et al., 2017) diagram for Otlakbaşı basaltic rocks. Three members used on the diagram taken from Oyan et al. (2017). SM – subducting sediment melts, SF – sediment derived fluids, AF – altered oceanic crust derived fluids, AOC – altered oceanic crust, PM – primitive mantle and UC – continental upper crust.

All this data indicates the presence of subduction components in less evolved samples from Otlakbaşı basaltic volcanism, and that these subduction components formed due to the effect of sediment melts dominantly with lower rates of fluids derived from sediments.

5.4. Partial Melting Process

To research and determine the partial melting processes for Otlakbaşı basaltic volcanism, partial melting models using rare earth elements (REE) were produced. During partial melting processes, REEs in source areas with spinel peridotite and/or garnet peridotite mineralogy have different solid-mineral/melt coefficients and thus behave differently and are very useful in conceptualising partial melt modelling. Melting processes in mantle source areas with garnet or spinel peridotite mineralogy initially enrich in light rare earth elements (LREE) and partial melting in the garnet peridotite facies produces slightly higher LREE/HREE ratios compared to melting in the spinel peridotite facies (Shaw et al., 2003). Additionally, MREE/HREE ratios only occur in the residual phase if there is garnet present ($^{Garnet\text{-}melt}D_{Yb} \sim 4$; $^{Garnet\text{-}melt}D_{MREE}$ ~0.21-1; McKenzie and O'Nions, 1991). This situation produces high MREE/HREE ratios in melts from mantle with garnet peridotite mineralogy, while contrarily partial melts from mantle source areas with spinel peridotite mineralogy have lower rates of MREE/HREE in melt fractionation and source and

melt ratios are similar ($^{Spinel-melt}D_{Yb}$ ~ 0.01; $^{Spinel-melt}D_{MREE}$ ~ 0.01; $^{Clinopyroxene-melt}D_{Yb}$ ~ 0.28; $^{Clinopyroxene-melt}D_{MREE}$ ~ 0.30; McKenzie and O'Nions, 1991). In light of this information, as the effects of partial melting of mantle with different source mineralogy varies in terms of REEs, they ensure clear observation of partial melting area and melting degree.

With the aim of determining partial melting processes of the Otlakbaşı basaltic rocks, partial melting was modelled using La/Yb against Tb/Yb element ratios. As shown in figure 11, the La/Yb – Th/Yb diagram illustrates 7 source areas with different mineralogies. Among these models are the phlogopite-rich garnet and spinel peridotite reflecting metasomatism effects, with amphibole-rich garnet and spinel peridotite curves. Partial melt modelling was created using nonmodal melting equations proposed by Shaw (1970). The parameters used in modelling are given in table 3. As seen on the diagram, only spinel and/or garnet-rich sources could not have formed the Otlakbaşı basaltic volcanism. Samples fall between the mixing curves obtained for different rates and degrees of melts from source areas with phlogopite- and/or amphibole-rich garnet peridotite and spinel peridotite mineralogy, with the condition that the spinel contribution is dominant. This modelling reveals that the Early Pliocene Otlakbaşı basaltic volcanism was produced from low partial melting degrees from residual mineral phase amphibole- and/or phlogopite-rich spinel peridotite mantle source area.

While fluids or sediment/AOC melts formed by subduction component effects enrich mantle source areas, residual phase minerals like amphibole and/or phlogopite are included in the mantle source area due to metasomatism processes. Considering the Otlakbaşı basaltic volcanism mantle source area was metasomatised by dominantly sediment melts with lesser rates of fluids, the question occurs of whether

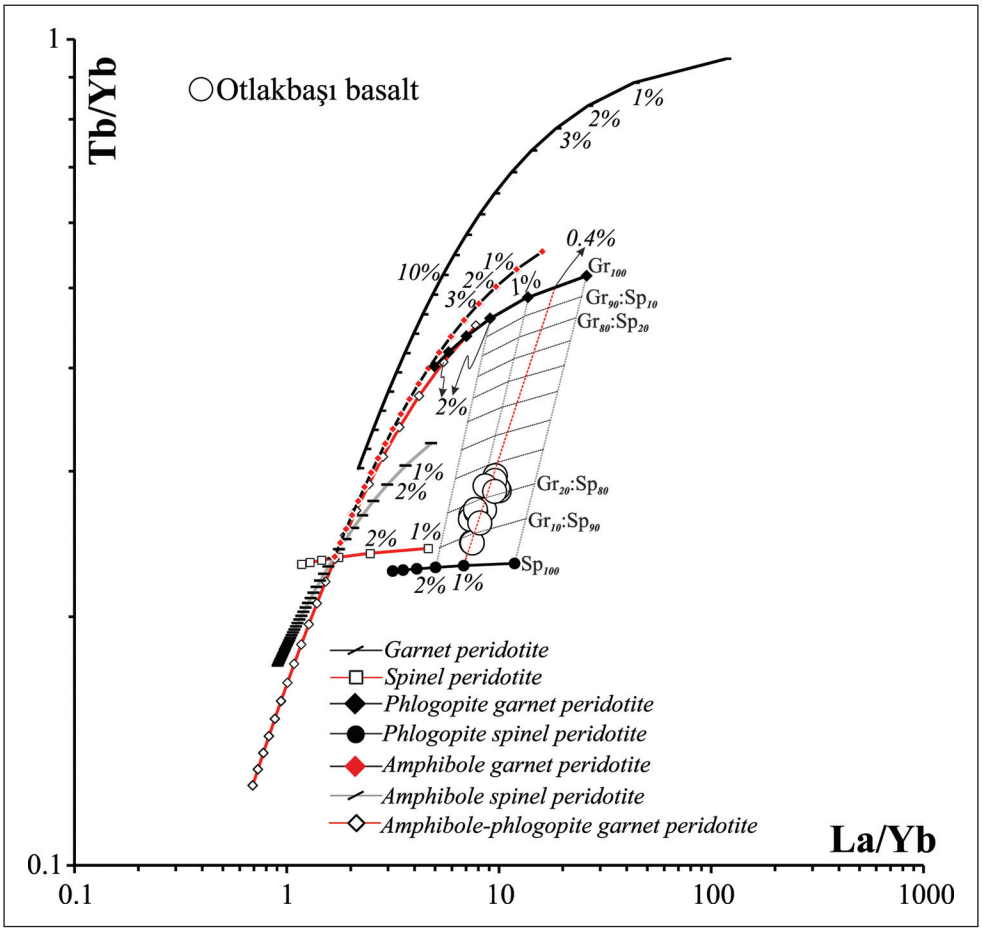

Figure 11- Partial melting model curves using La/Yb-Tb/Yb element ratios. The mineralogy and parameters used in modelling are given in table 2. To reduce AFC process effects to a minimum, samples were drawn after confirming 8% MgO value fractionation.

Table 3- Parameters used in non-modal mass balance melting given in figure 11. Discriminant coefficients taken from McKenzie and O'Nions (1992), Ionov et al. (2002) and Adam and Green (2006). Source mode and melt mode mineralogic compositions taken from Oyan et al. (2017).

	Olivine	*Orthopyroxene*	*Clinopyroxene*	*Spinel*	*Garnet*	*Amphibole*	*Phlogopite*	*Total*
	Garnet peridotite (PM source)[1]							
Source mode	0.598	0.211	0.076		0.115			1
Melt mode	0.05	0.2	0.3		0.45			1
	Amphibole garnet peridotite (PM source)[5]							
Source mode	0.794	0.123	0.03		0.011	0.042		1
Melt mode	0.15	0.15	0.22		0.15	0.33		1
	Phlogopite garnet peridotite (PM source)[5]							
Source mode	0.55	0.22	0.15		0.03		0.05	1
Melt mode	0.05	0.05	0.65		0.05		0.20	1
	Amphibole phlogopite garnet peridotite (PM source)[4]							
Source mode	0.55	0.20	0.15		0.05	0.04	0.01	1
Melt mode	0.05	0.05	0.20		0.20	0.40	0.10	1
	Spinel peridotite (PM source)[1]							
Source mode	0.578	0.27	0.119	0.033				1
Melt mode	0.10	0.27	0.5	0.13				1
	Phlogopite spinel peridotite (PM source)[5]							
Source mode	0.48	0.30	0.18	0.02			0.02	1
Melt mode	0.10	0.35	0.47	0.02			0.06	1
	Amphibole spinel peridotite (PM source)[3]							
Source mode	0.794	0.123	0.03	0.011		0.042		1
Melt mode	0.15	0.15	0.22	0.06		0.42		1

amphibole and/or phlogopite were present in the mantle source area. The answer to this question may be identified from the variation in trace element chemistry of the rocks. As K element is highly compatible with phlogopite and amphibole, if these minerals are present in the mantle wedge as residual phase in partial melting processes, then at low partial melting degrees K element is held by these minerals and does not enrich in the melt. With the increase in the degree of partial melt, the melt begins to enrich in K in direct correlation with the consumption of residual mineral phases in the source area. If these minerals are not present in the mantle wedge, dry melt conditions are present and K acts highly incompatibly and remains fixed with the variation in melting degree. In light of this information, to test whether residual mineral phase melting occurred in the mantle source area of the Otlakbaşı basaltic lava, K/K* (K anomaly) – La/Yb binary variation diagrams were produced (Figure 12). On this diagram, there is a negative trend with the increasing partial melt degrees for Otlakbaşı basaltic lava. This negative trend shows there may have been

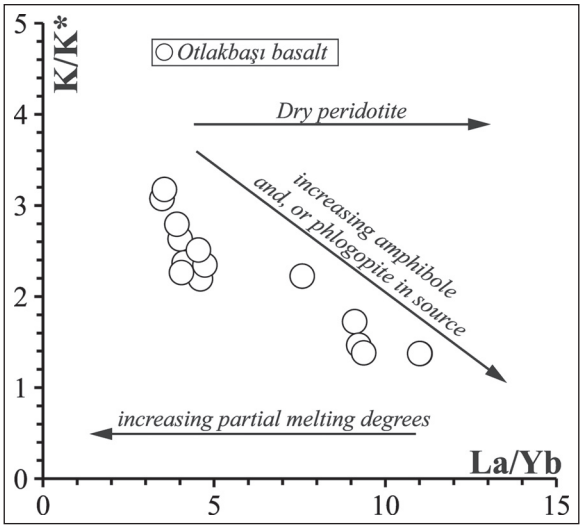

Figure 12- La/Yb against K/K* variation diagram for Otlakbaşı basaltic lava [$K/K^*=K_{PM}$ / $(Nb_{PM}*Th_{PM})^{½}$; PM values normalised to primitive mantle]. Falling partial melting degrees in basaltic lava towards positive K/K* values. This data is associated with the presence of phlogopite or amphibole in the mantle source area. To reduce AFC process effects to a minimum, samples were drawn after confirming 8% MgO value fractionation.

aqueous minerals like phlogopite and/or amphibole in the source area as residual mineral phase.

For samples from the Otlakbaşı basaltic volcanism considered less evolved and not affected by AFC processes, primitive mantle normalised multielement spider diagrams show depletion of Ba compared to Rb indicating phlogopite was more dominant in the source area compared to amphibole. The most important reason for this is that phlogopite has higher discriminant coefficient for Ba compared to Rb compared to amphibole (Green and Ringwood, 1967). With the aim of determining the presence of phlogopite or amphibole in the mantle source area, primitive mantle normalised Ba/Rb – Rb/Sr binary variation diagrams were created. Ba, Rb and Sr have different discriminant coefficients for amphibole and phlogopite, so elevated Ba/Rb and low Rb/Sr element ratios reflect the traces of amphibole while high Rb/Sr and low Ba/Rb ratios reflect phlogopite. Additionally, Sr has higher discriminant coefficient values for amphibole compared to phlogopite. As seen on figure 13, falling Ba/Rb and increasing Rb/Sr values for lava from Otlakbaşı basaltic volcanism indicates the possible presence of typical phlogopite in the mantle source area.

Alternatively, the variation in the ratios of incompatible elements of Ba and Rb in Otlakbaşı basaltic rock samples may be caused by exposure to fractional crystallisation of phlogopite in the magma chamber. With the aim of revealing these effects, the solidification index of MgO values against primitive mantle normalised Ba/Rb ratio diagrams were produced. As seen in figure 13b, there was no good correlation observed between MgO values and Ba/Rb_{PM} values and this situation reveals that phlogopite did not crystallise during magma chamber evolution processes. As a result, the presence of phlogopite appears not to be related to the magma chamber but may be related to metasomatisation processes in the mantle source area.

Experimental melt results for phlogopite-rich peridotite (spinel or garnet) source have revealed a phase with phlogopite, forsterite, hypersthene, diopside, spinel and steam (phlogopite spinel lherzolite) forming at nearly 15 kbar pressure and nearly 1000 ºC and equilibrium fluid contains 0.5 to 1% K_2O content (thus low alkali and low potassic). But at 30 kbar pressure and nearly 1100-1200 ºC, the fluid in equilibrium with phlogopite, forsterite, hypersthene, diopside, garnet and steam (phlogopite garnet lherzolite) phase had nearly 2.5% K_2O content (thus alkali, possibly high, and high potassic) (Bravo and O'Hara, 1975). When it is considered that Otlakbaşı lava derived from a spinel peridotite dominant mineralogy with melting in shallow conditions (nearly 50-60 km, 15-20 kbar), it supports the view that alkali rates in the experimental data may not be very high. An experimental study by Condamine et al. (2016) stated that phlogopite-rich silica-saturated lavas may produce high K lava and the melt formed in this situation will have silica amounts from 52-63%. However, this study also showed that in experimental conditions melting of a phlogopite-rich spinel peridotite source may not contain phlogopite in the melt phase but may contain olivine and pyroxene with spinel. In this situation, as phlogopite does not enter the melt, the K amounts may remain low. If there is phlogopite in the residual mineral phase

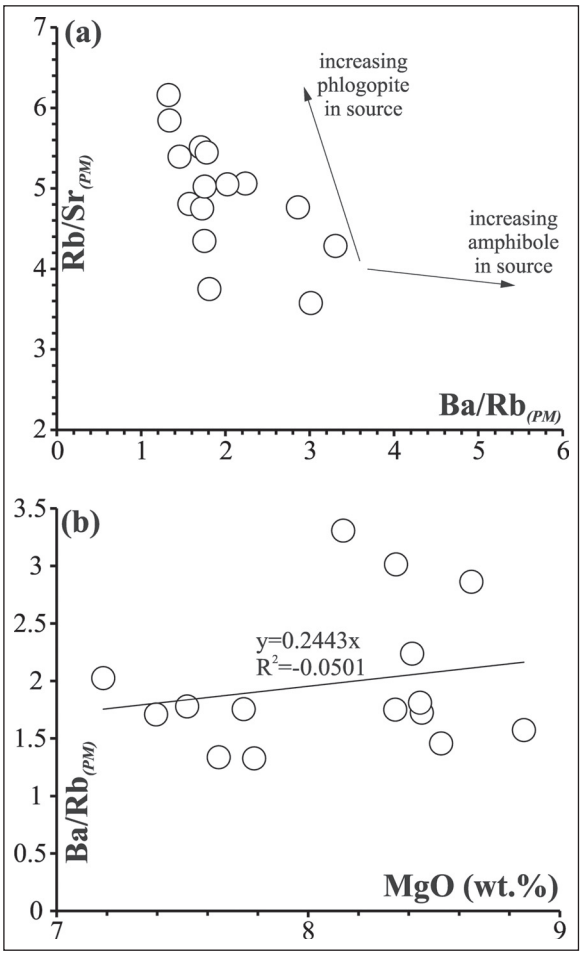

Figure 13- a) Variation of Rb/Sr trace element ratios normalised to primitive mantle (Furham and Graham, 1999), b) Ba/Rb trace element ratios normalised to primitive mantle against MgO.

during production of tholeiitic melts, phlogopite will have a tendency to buffer the K concentration in the melt and then K and Rb elements may display compatible behaviour in the magmatic system rather than incompatible behaviour (Hofmann and Hart, 1978). Additionally, if the amount of phlogopite in the source is greater than the amount in melt, then low partial melting degrees will leave phlogopite as residual phase in the source; thus, the K content of the melt may be low. All this data supports the view that phlogopite and/or amphibole existed as residual mineral phase in the mantle source area for Otlakbaşı basaltic volcanism and that phlogopite may have been more dominant compared to amphibole.

5.5. Geodynamics

Nearly 2/3 of the EACZ is covered with young volcanic rocks (from Miocene to historical periods) and is mean ~2 km above sea level (Şengör et al., 2008). With compression-contraction tectonic regime dominant until the Late Miocene-Early Pliocene, the EACZ entered a compression-extensional tectonic regime in the Early-Late Pliocene (Koçyiğit et al., 2001). Though different geodynamic models have been proposed for the EACZ by many researchers (Innocenti et al., 1982; Pearce et al., 1990; Yılmaz et al., 1998; Keskin 2003 and 2007; Şengör et al., 2008), the most important of these models may be summarised as partial delamination of lithospheric mantle (Pearce et al., 1990; Oyan et al., 2016, 2017), steepening and breaking of subducting oceanic lithosphere (Keskin, 2003; Şengör et al., 2008) or regional-scale broad volcanism as a result of elevation of enriched asthenospheric mantle.

Latest studies about the source area and root of intense volcanic activity in the region have focused on mixture of different melt degrees and different proportions of asthenospheric and lithospheric mantle to form the volcanism (Özdemir and Güleç, 2014; Oyan et al., 2016). Quaternary volcanism north of Lake Van was determined to have formed from amphibole-rich garnet peridotite melt and delamination of the lithospheric mantle may have been responsible for this (Pearce et al., 1990; Oyan et al., 2016). Studies of volcanism in the region indicate a mantle source area with EM2 type enrichment of isotopic and trace element concentrations in most primitive lava and the presence of significant amounts of subduction components (Pearce et al., 1990; Yılmaz et al., 1998; Keskin et al., 1998; Keskin, 2003; Özdemir et al., 2006; Özdemir and Güleç, 2014; Oyan et al., 2016, 2017). The majority of these studies mention the presence of subduction components, while Oyan et al. (2016, 2017) revealed that subduction components derived from sediment melts and metasomatisation processes were dominant in nearly 2 to 10% of sediment melts, based on petrologic modelling. This data may explain the regional-scale volcanism processes as a mixture of lithospheric and asthenospheric mantle via lithospheric delamination and clear metasomatisation of sediment melts in lithospheric mantle.

Geophysical studies with the aim of determining the crustal structure of the EACZ have reported that there is no or very thin lithospheric mantle below the region; as a result, the EAAC sits directly on asthenospheric mantle (Al-Lazki et al., 2003; Gök et al., 2003; Sandvol et al., 2003). Additionally, Angus et al. (2006) and Özacar et al. (2008) indicated there may be 70-80 km thickness of lithosphere below the region. When it is considered the crust below the EACZ has mean 45 km thickness (Zor et al., 2003), it may be that there is 30-35 km thin lithospheric mantle below the region. Partial melting models of Otlakbaşı basaltic volcanism indicate the presence of spinel-rich mantle in the source area of these lavas. Considering the spinel and garnet transition zone is nearly 80 km depth (Takahashi and Kushiro, 1983), it is understood the spinel-rich mantle source for the EACZ derived from lithospheric mantle. Oyan et al. (2016) studied the Pliocene basaltic rocks in the region and found lavas forming broad plateaus erupted in a narrow time interval of 4.9 to 4.5 My, with character transitioning from alkali to subalkali and an increase in spinel peridotite melts over time. This data is compatible with melt results for the Pliocene-aged Otlakbaşı basaltic lava. Data support the opinion that the source area forming the volcanism formed from partial melting of spinel-rich lithospheric mantle and metasomatised zones containing dominantly phlogopite over amphibole.

6. Conclusion

The Otlakbaşı volcanism located east of Lake Van has different output centres and basaltic composition. Ar-Ar dating results indicate this volcanism erupted in the Early Pliocene-Zanclean (4.14 My), contrary to the known age of Quaternary. Petrologic modelling completed with the aim of determining magma chamber evolution reveal that continental contamination was effective in the magma chamber

of this volcanism, though fractional crystallisation effects were slightly less than crustal contamination.

The primitive mantle-normalised trace element characteristics of the least evolved rock samples from the Otlakbaşı basaltic volcanism were determined to be clearly depleted in HFSE elements compared to LILE and LREE elements and enriched in Pb compared to neighbouring elements. This finding shows enrichment of the mantle source area in terms of subduction components. Subduction components came from dominantly sediment melts and fluids from sediments to a lesser extent.

Melt modelling to determine the nature of the mantle source area indicate the source forming this basaltic volcanism may have formed from dominantly metasomatised 1% spinel peridotite facies melts. Delamination of lithospheric mantle within the EACZ with metasomatised spinel-rich melts in shallow zones in the lithospheric mantle may be responsible for the Otlakbaşı basaltic volcanism in the Pliocene period.

Acknowledgements

This study was supported by Van Yüzüncü Yıl University SRP project number 2012- HIZ-MİM001 and TÜBİTAK project number 113Y406. The author wishes to thank Dr. İrfan Temizel, Dr. Fatih Karaoğlan, Dr. Kurtuluş Günay and anonymous reviewers for contributing their constructive criticism and opinions of the manuscript.

References

Acarlar, M., Erkal, T., Güner, E., Şen, A., Umut, M., Elibjol, E., Gedik, İ., Hakyemez, Y., Uğuz, F. 1991. Van Gölü Doğu ve Kuzeyinin Jeolojisi, Maden Tetkik ve Arama Genel Müdürlüğü, Rapor No: 9469, 94 s. Ankara (unpublished).

Adam, J., Green, T. 2006. Trace element partitioning between mica- and amphibole-bearing garnet lherzolite and hydrous basanitic melt: 1. Experimental results and the investigation of controls on partitioning behavior. Contributions to Mineralogy and Petrology 152, 1-17.

Aldanmaz, E., Yalınız, M.K., Güçtekin, A., Göncüoğlu, M.C. 2007. Geochemical characteristics of mafic lavas from the Neotethyan ophiolites in western Turkey: implications for heterogeneous source contribution during variable stages of ocean crust generation. Geological Magazine 145, 37-54.

Al-Lazki, A., Seber, D., Sandvol, E., Türkelli, N., Mohamad, R., Barazangi, M. 2003. Tomographic Pn velocity and anisotropy structure beneath the Anatolian plateau (eastern Turkey) and the surrounding regions, Geophysical Research Letter 30, 8043.

Allen, M., Armstrong, H. A. 2008. Arabia-Eurasia collision and the forcing of mid-Cenozoic global cooling. Palaeogeography, Palaeoclimatology, Palaeoecology 265, 52-58.

Angus, D.A., Wilson, D.C., Sandvol, E., Ni, J.F. 2006. Lithospheric structure of the Arabian and Eurasian collision zone in Eastern Turkey from S-wave receiver functions. Geophysical Journal of International 166, 1335-1346.

Bağcı, U., Alpaslan, M., Frei, R., Kurt, M.A., Temel, A. 2011. Different Degrees of Partial Melting of the Enriched Mantle Source for Plio-Quaternary Basic Volcanism, Toprakkale (Osmaniye) region, Southern Turkey. Turkish Journal of Earth Science 20, 115-135.

Bravo, M.S., O'Hara, M.J. 1975. Partial melting of phlogopite–bearing synthetic spinel– and garnet–lherzolites. Physics and Chemistry of the Earth 54, 845-854.

Class, C., Miller, D. M., Goldstein, S. L., Langmuir, C. H. 2000. Distinguishing melt and fluid subduction components in Umnak volcanics: Aleutian arc. Geochemistry, Geophysics, Geosystems (3G) 1, 1-34.

Condamine, P., Medard, E., Devidal, J.L. 2016. Experimental melting of phlogopite-peridotite in the garnet stability field. Contribution to mineralogy and petrology 95, 1-26.

DePaolo, D. J. 1981. Trace element and isotopic effects of combined wall-rock assimilation and fractional crystallization. Earth and Planetary Science Letters 53, 189–202.

Elburg, M. A., Bergen, M. V., Hoogewerff, J., Foden, J., Vroon, P., Zulkarnain, I., Nasution, A. 2002. Geochemical trends across an arc–continent collision zone: magma sources and slab–wedge transfer processes below the Pantar Strait volcanoes, Indonesia. Geochimica et Cosmochimica Acta 66, 2771–2789.

Elliott, T., Planck, T., Zindler, A., White, W., Bourdon, B. 1997. Element transport from slab to volcanic front at the Mariana arc. Journal of Geophysical Research 102, 14991–15019.

Foley, S. F., Tiepolo, M., Vannucci, R. 2002. Growth of early continental crust controlled by melting of amphibolite in subduction zones. Nature 417, 837– 840.

Furham, T., Graham, D. 1999. Erosion of lithospheric mantle beneath the East African Rift system: geochemical evidence from the Kivu volcanic province. Lithos, 48, 237-262.

Green, D. H., Ringwood, A. E. 1967. The stability fields of aluminous pyroxene peridotite and garnet peridotite. Earth and Planetary Science Letters 3, 151-160.

Göğüş, O. H., Pysklywec, R. N. 2008. Mantle lithosphere delamination driving plateau uplift and synconvergent extension in eastern Anatolia. Geology 36, 723-726.

Gök, R., Sandvol, E., Türkelli, N., Seber, D., Barazangi, M. 2003. Sn attenuation in the Anatolian and Iranian plateau and surrounding regions, Geophysical Research Letter 30, 8038 -8042.

Hawkesworth, C. J., Turner, S. P., McDermott, F., Peate, D. W., Van Calsteren, P. 1997. U–Th isotopes in arc magmas: implications for element transfer from the subducted crust. Science 276, 551–555.

Hofmann, A.W., Hart, S. 1978. An assessment of local and regional ısotopic equilibrıum in the mantle. Earth and Planetary Science Letters 38, 44-62.

Innocenti, F., Mazzuoli, R., Pasquaré, G., Radicati di Brozolo, F., Villari, L. 1982. Tertiary and Quaternary volcanism of the Erzurum-Kars area (Eastern Turkey): Geochronological data and geodynamic evolution. Journal of Volcanology and Geothermal Research 13, 223-240.

Irvine, T. N., Baragar, W. R. A. 1971. A guide to the chemical classification of the common volcanic rocks. Canadian Journal of.Earth Sciences 8, 523-548.

Ionov, D.A., Bodinier, J.-L.,Mukasa, S.B. Zanetti, A. 2002. Mechanisms and sources of mantle metasomatism: major and trace element compositions of peridotite xenoliths from Spitsbergen in the context of numerical modelling. Journal of Petrology 43, 2219–2259.

Karaoğlan, F., Parlak, O., Thöni, M., Klötzli, U., Koller, F. 2016. The temporal evolution of the active margin along the Southeast Anatolian Orogenic Belt (SE Turkey): Evidence from U–Pb, Ar–Ar and fission track chronology. Gondwana Research 33, 190-208.

Karapetian, S.G., Jrbashian, R.T., Mnatsakanian, A.K. 2001. Late collision rhyolitic volcanism in the north-eastern part of the Armenian Highland, Journal of Volcanology and Geothermal Research 112, 189-220.

Keskin, M. 2003. Magma generation by slab steepening and breakoff beneath a subduction-accretion complex: An alternative model for collision-related volcanism in Eastern Anatolia, Turkey. Geophysical Research Letters 30, 8046-8050.

Keskin, M., 2007. Eastern Anatolia: a hot spot in a collision zone without a mantle pluma. In:Foulger, G.R., and Jurdy, D., (eds) Plates, Plumes and Planetary Processes. Geological Society of America, Special papers 430, 693-722.

Keskin, M., Pearce, J. A., Mitchell, J. G. 1998. Volcano-stratigraphy and geochemistry of collision-related volcanism on the Erzurum-Kars Plateau, North Eastern Turkey. Journal of Volcanology and Geothermal Research 85, 355-404.

Keskin, M., Genç, Ş. C., Aysal, N., Özeren, M. S., Sharkov, E. V., Lebedev, V. A., Chugaev, A. V., Oyan, V., Özdemir, Y., Ünal, E., Karaoğlu, Ö., Duru, O., 2013. Tectono-magmatic processes across the Arabian-Eurasian collision zone and their geodynamic significance: an integrated geological, petrological, geochemical and geochronological study of the post-collisional Cenozoic volcanic units displaying a transition from orogenic to anorogenic nature across a geotraverse from Caucasus to Arabian foreland, Unpublished report of TÜBİTAK-RFBR project #108Y222.

Kessel, R., Schmidt, M., Ulmer, P., Pettke, T. 2005. Trace element signature of subduction-zone fluids, melts and supercritical liquids at 120-180 km depth. Nature 437, 724-727.

Koçyiğit, A., Yılmaz, A., Adamia, S., Kuloshvili, S. 2001. Neotectonics of East Anatolian plateau (Turkey) and lesser caucasus: Implication for transition from thrusting to strike-slip faulting. Geodinamica Acta 14, 177-195.

Krienitz, M. S., Haase, K.M., Mezger, K., Eckardt, V., Shaikh-Mashail, M. A. 2006. Magma genesis and crustal contamination of continental intraplate lavas in northwestern Syria. Contribution of Mineralogy and Petrology 151, 698–716.

Le Bas, M.J., Le Maitre, R.W., Streckeisen, A., Zanettin, B. 1986. A chemical classification of volcanic rocks based on the total alkali-silica diagram. Journal of Petrology 27, 745–750.

Lebedev, V.A., Sharkov, E.V., Keskin, M., Oyan, V. 2010. Geochronology of the Late Cenozoic volcanism in the area of Van Lake (Turkey): an example of the developmental dynamics for magmatic processes. Doklady Earth Sciences 433, 1031–1037.

Lustrino, M., Wilson, M. 2007. The circum-Mediterranean anorogenic Cenozoic igneous province. Earth Science Reviews 81, 1-65.

Mc Kenzie, D. P., O'Nions, R. K. 1991. Partial melt distributions from inversion of rare earth element concentrations. Journal of Petrology 32, 1021-1091.

MTA. 2008. 1/100000 ölçekli Başkale K-51 paftası. Maden Tetkik ve Arama Genel Müdürlüğü, Ankara.

Okay, A. I., Zattin, M., Cavazza, W. 2010. Apatite fission-track data for the Miocene Arabian-Eurasia collision. Geology 38, 35-38.

Oyan, V. 2011. Vocanostratigraphy, Petrology and Magmatic Evolution of the Etrusk Volcano and Surrounding Areas (North of Lake Van, Turkey). PhD thesis, Yüzüncü Yıl Universtiy, 362 s.Van, Turkey.

Oyan, V., Keskin, M., Lebedev, V.A., Chugaev, A.V., Sharkov, E.V. 2016. Magmatic evolution of the Early Pliocene Etrüsk stratovolcano, Eastern Anatolia collision zone, Turkey. Lithos 256-257, 88-108.

Oyan, V., Keskin, M., Lebedev, V.A., Chugaev, A.V., Sharkov, E.V., Ünal, E. 2017. Petrology and Geochemistry of the Quaternary Mafic Volcanism in the northeast of Lake Van, Eastern Anatolian Collision Zone, Turkey. Journal of Petrology DOI: https://doi.org/10.1093/petrology/egx070.

Özacar, A.A., Gilbert, H., Zandt, G. 2008. Upper mantle discontinuity structure beneath East Anatolian Plateau (Turkey) from receiver functions. Earth and Planetary Science Letters 269, 426-434.

Özdemir, Y., Karaoğlu, Ö., Tolluoğlu, A.Ü., Güleç, N. 2006. Volcanostratigraphy and petrogenesis of the Nemrut stratovolcano (East Anatolia High Plateau): The most recent post-collisional volcanism in Turkey. Chemical Geology 226, 189-211.

Özdemir, Y., Güleç, N. 2014. Geological and Geochemical evoluation of Suphan Stratovolcano Eastern Anatolia, Turkey: Evidence for the lithosphere-asthenosphere interaction on post collisional volcanism. Journal of Petrology 55, 37-62.

Parlak, O., Delaloye, M., Kozlu, H., Fontıgnie, D. 2000. Trace element and Sr-Nd isotope geochemistry of the alkali basalts observed along the Yumurtalık Fault (Adana) in southern Turkey. Yerbilimleri 22, 137-148.

Pearce, J.A., Bender, J.F., De Long, S.E., Kidd, W.S.F., Low, P.J., Güner, Y., Şaroğlu, F., Yılmaz, Y., Moorbath, S., Mitchell, J.G. 1990. Genesis of collision volcanism in Eastern Anatolia, Turkey. Journal of Volcanol and Geothermal Research 44, 189-229.

Pearce, J.A., Stern.R.J., Bloomer, H.S., Fryer, P. 2005. Geochemical mapping of the Mariana arc-basin system: Implications for the nature and distribution of subduction components. Geochemistry, Geophysics, Geosystem (3G*)* 6, 1-27.

Plank, T., Langmuir, C. H. 1998. The chemical composition of subducting sediment and its consequences for the crust and mantle. Chemical Geology 145, 325–394.

Peccerillo, A., Taylor, S.R., 1976. Geochemistry of Eocene calc-alkaline volcanic rocks from the Kastamonu area. Northern Turkey. Contributions to Mineralogy and Petrology 58 63–81.

Sandvol, E., Türkelli, N., Barazangi, M. 2003. The Eastern Turkey Seismic Experiment: The study of a young continent-continent collision. Geophysical Research Letter 24, 8038-8041.

Shaw, J.E., Baker, J.A., Menzies, M.A., Thirlwall, M.F., İbrahim, K.M. 2003. Petrogenesis of the largest intraplate volcanic field on the Arabian Plate (Jordan): a mixed lithosphere–asthenosphere source activated by lithospheric extension. Journal of Petrology 44, 1657– 1679.

Staudacher,Th., Jessberger, E. K., Dorflinger, D., Kiko, J. 1978. A refined ultra-high vacuum furnace for rare gas analysis. Journal of Physics E: Scientific Instruments 11,781-784.

Şengör, A.M.C., Kidd, W.S.F. 1979. Post – collisional tectonics of the Turkısh – Iranian plateau and a comparison with tibet. Tectonophysisics 55, 361-376.

Şengör, A.M.C., Özeren, M.S., Keskin, M., Sakınç, M., Özbakır, A.D., Kayan, I. 2008. Eastern Turkish high plateau as a small Turkic-type orogen: implications for post-collisional crust-forming processes in Turkic-type orogens. Earth Science Reviews 90, 1-48.

Schildgen, T.F., Yildirim, C., Cosentino, D., Strecker, M.R. 2014. Linking slab break-off, Hellenic trench retreat, and uplift of the central and Eastern Anatolian plateaus. Earth Science Reviews 128, 147–168.

Shaw, D.M. 1970. Trace element fractionation during anatexis. Geochimica et Cosmochimica Acta 34, 237-243.

Sun, S.S., McDonough, W.F. 1989. Chemical and isotopic systematics of oceanic basalts: implications for mantle composition and processes. In: Saunders, A.D. & Norry, M.J. (ed.) In Magmatism in Ocean Basins, Geological Society of London Special Publication 42, 313-345.

Takahashi, E., Kushiro, I. 1983. Melting of a dry peridotite at high pressures and basalt magma genesis. American Mineralogist 68, 859-879.

Tatsumi, Y., Hamilton, D.J., Nesbitt, R. W. 1986. Chemical characterization of fluid phase released from a subducted lithosphere and origin of arc magmas: Evidence from high-pressure experiments and natural rocks. Journal of Volcanology and Geothermal Research 29, 293–309.

Taylor, S.R., McLennan, S.M. 1985. The continental crust: its composition and evolution, Geoscience Texts. Blackwell Scientific Publications, London.

Topuz, G., Altherr, R., Kalt, A., Satır, M., Werner, O., Schwarz, W.H. 2004. Aluminous granulites from the Pulur complex, NE Turkey: a case of partial melting, efficient melt extraction and crystallization, Lithos 72, 183-207.

Turner, S. P. 2002. On the time-scales of magmatism at island-arc volcanoes. Philosophical Transactions of the Royal Society of London, Mathematical, Physical and Engineering Sciences 360, 2853–2871.

Yılmaz, Y., Şaroğlu, F., Güner, Y. 1987. Initation of the neomagmatism in East Anatolia. Tectonophysics 137, 177-199.

Yılmaz, Y., Güner, Y., Şaroğlu, F. 1998. Geology of the Quaternary volcanic centres of the East Anatolia. Journal of Volcanology and Geothermal Research 85,173-210.

Zor, E., Gürbüz, C., Türkelli, N., Sandvol, E., Seber, D., Barazangi, M. 2003. The crustal structure of the East Anatolian Plateau from receiver functions. Geophysical Research Letters 30, 8044-8047.